

# Kinetics of the CHCl<sub>2</sub> and CH<sub>2</sub>Cl Association Reactions with Molecular Oxygen between 298 and 448 K and from 1 to 760 Torr of Total Pressure

Frederick F. Fenter,\* Phillip D. Lightfoot,† Françoise Caralp, and Robert Lesclaux

Laboratoire de Photophysique et Photochimie Moléculaire, Université de Bordeaux I, 351 Cours de la Libération, 33405 Talence Cedex, France

Jukka T. Niiranen‡ and David Gutman

Department of Chemistry, Catholic University of America, Washington, DC 20064

Received: December 26, 1992

The rate constants for the recombination reactions between molecular oxygen and the halogenated methyl radicals CHCl<sub>2</sub> and CH<sub>2</sub>Cl were determined over the pressure range of 1 to 760 Torr in nitrogen as a function of temperature. The CHCl<sub>2</sub> + O<sub>2</sub> reaction (1) was studied over the temperature range 298 < T/K < 383 and the CH<sub>2</sub>Cl reaction (2) over the range 298 < T/K < 448. The large range in pressure was attained by using two complementary techniques: Low-pressure experiments (1–10 Torr) were concluded using laser photolysis/photoionization mass spectrometry. High-pressure experiments (20–760 Torr) were carried out with the laser photolysis/UV absorption spectroscopy technique. A nonvariational RRKM calculation using previously determined thermodynamic parameters for these two reactions was performed, providing a complete and coherent picture of the kinetics and equilibria for these reactions. In addition, the data were fitted to a simplified and commonly used form of an expression developed by Troe to extrapolate falloff data to obtain high- and low-pressure limiting rate constants. Parameters are provided that allow the calculation of the rate constants of the title reactions as a function of temperature and pressure. The data are well represented by the following limiting rate-constant expressions: reaction 1,  $k_o(T) = (1.26 \pm 0.03) \times 10^{-30}(T/300)^{-4.0 \pm 0.2} \text{ cm}^6 \text{ molecule}^{-2} \text{ s}^{-1}$ ,  $k_{oo}(T) = (2.8 \pm 0.2) \times 10^{-12}(T/300)^{-1.4 \pm 0.3} \text{ cm}^3 \text{ molecule}^{-1} \text{ s}^{-1}$ ; reaction 2,  $k_o(T) = (1.88 \pm 0.05) \times 10^{-30}(T/300)^{-3.2 \pm 0.2} \text{ cm}^6 \text{ molecule}^{-2} \text{ s}^{-1}$ ,  $k_{oo}(T) = (2.9 \pm 0.2) \times 10^{-12}(T/300)^{-1.2 \pm 0.4} \text{ cm}^3 \text{ molecule}^{-1} \text{ s}^{-1}$ .

## Introduction

Chlorinated alkyl radicals are formed in a number of chemical environments as intermediate species in the oxidation of halogenated hydrocarbons.<sup>1,2</sup> In the atmosphere, where these radicals represent an important source of chlorine, the pathway of their subsequent oxidation is a process of practical interest.<sup>1</sup> In particular, a key elementary reaction of polyatomic free radicals in the atmosphere is oxidation by molecular oxygen. Within the family of chlorinated alkyl radicals, very little kinetic information on the recombination of these species with O<sub>2</sub> is available. Of the chlorinated methyl radicals, for example, only the fully substituted species CCl<sub>3</sub> has been well studied; the rate constant for the reaction of CCl<sub>3</sub> + O<sub>2</sub> has been determined over a moderately broad range of temperature and pressure,<sup>3–7</sup> and the equilibrium constant for the process has been determined.<sup>8</sup> In addition, the reaction of the fluorinated radical CCl<sub>2</sub>F with O<sub>2</sub> has been studied at pressures below 10 Torr.<sup>9</sup> For the partially chlorinated methyl radicals, no kinetic information is available; however, the equilibrium constants for the reactions of CHCl<sub>2</sub> and CH<sub>2</sub>Cl with O<sub>2</sub> have been recently determined by Russell et al.<sup>10</sup>

This work is part of a general effort to determine the rate constants for the association reactions of halogenated alkyl radicals with O<sub>2</sub> over a large range of pressure as a function of temperature. In this study, we present our results on the recombination reactions of the CHCl<sub>2</sub> and the CH<sub>2</sub>Cl radicals with molecular oxygen:



A large range in experimental pressures is obtained by using two complementary techniques. The low-pressure rate constants, for pressures between 1 and 10 Torr, were determined by experiments using the laser photolysis/photoionization mass spectrometry technique. High-pressure rate constants were determined for the pressure range 20–760 Torr by the technique laser photolysis/UV absorption spectroscopy. We recently reported our results on the CCl<sub>3</sub> + O<sub>2</sub> reaction, where we demonstrated the feasibility of using these two complementary methods to obtain kinetic data over a broad range of pressure.<sup>7</sup>

## Experimental Details

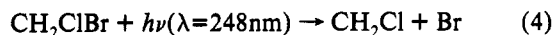
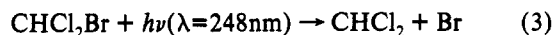
The pressure dependence of the rate constant for reaction 1 was measured at the temperatures 298, 333, and 383 K, and reaction 2 was studied at these as well as at a fourth temperature of 448 K, using two time-resolved techniques covering complementary ranges in pressure. These two experimental techniques are discussed separately below.

**A. Study Using Photoionization Mass Spectrometric Detection.** The apparatus and its use to determine R + O<sub>2</sub> rate constants has already been described in detail.<sup>11,12</sup> Only a brief summary is presented for this discussion. The reactor is a heatable, 1.05-cm-i.d. uncoated quartz tube coupled to a photoionization mass spectrometer. Gas flowing through the reactor (at ca. 5 ms<sup>-1</sup>) contained the radical precursor in very low concentrations (typically 0.01%), O<sub>2</sub> in varying amounts (0.1–10%), and the carrier gas (N<sub>2</sub> or He). In view of the significant contribution of oxygen to the total pressure under some conditions, nitrogen was used as the carrier gas for most of the experiments as N<sub>2</sub> and O<sub>2</sub> have much more similar collisional efficiencies than He and O<sub>2</sub>.<sup>13</sup> Pulsed (5 Hz) unfocused 248-nm radiation from a Lambda Physik EMG 201 MSC excimer laser was collimated and then

\* Current address: Group Technical Centre, ICI Explosives, McMasterville, Quebec, Canada J3G 1T9.

† Current address: Department of Physical Chemistry, University of Helsinki, Meritullinkatu IC, SF-00170 Helsinki, Finland.

directed along the axis of the tube. The laser fluence was varied using quartz flats or wire screens placed between the laser and the reactor.  $\text{CHCl}_2$  and  $\text{CH}_2\text{Cl}$  were produced uniformly along the reactor by the photolysis of the corresponding bromide:



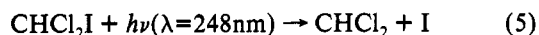
The extent of photolysis was too small to measure experimentally (i.e.,  $<0.5\%$ ), resulting in an upper limit for the initial radical concentration of  $1 \times 10^{11}$  molecules  $\text{cm}^{-3}$ . This ensured that radical-radical reactions were unimportant in these experiments and that the only significant loss processes for the alkyl radicals were reaction with  $\text{O}_2$  and loss on the walls.

Gas was sampled through a 0.4-mm-diameter hole, located at the end of a nozzle in the wall of the reactor, and formed into a beam by a conical skimmer before entering a vacuum chamber containing the photoionization mass spectrometer. As the beam traversed the ion source, a portion was photoionized and then mass selected.  $\text{CHCl}_2$  and  $\text{CH}_2\text{Cl}$  were photoionized by 8.9–9.1-eV radiation,  $\text{CHCl}_2\text{Br}$  and  $\text{CH}_2\text{ClBr}$  by 11.6–11.8-eV radiation. Mass-selected ion signals were collected from a short time before the laser pulse until up to 26 ms afterward, using a multichannel scaler. Data from 1000 to 15 000 laser shots were accumulated for acceptable signal-to-noise ratios.

The radical precursors,  $\text{CHCl}_2\text{Br}$  (Aldrich, purity  $>98\%$ ) and  $\text{CH}_2\text{ClBr}$  (Aldrich, purity of  $99\%$ ), were degassed before use; oxygen (Matheson, extra dray, purity of  $99.6\%$ ), nitrogen (Matheson, purity of  $99.995\%$ ), and helium (Matheson, purity of  $99.995\%$ ) were each used as supplied.

**B. Study Using Ultraviolet Absorption Spectrometric Detection.** The apparatus used for these experiments was described in our study of the  $\text{CCl}_3 + \text{O}_2$  reaction;<sup>7</sup> an abbreviated description follows. The apparatus consists of an oven-mounted cell, 80 cm in length, which is made of 11-mm-i.d. Pyrex tubing with spectroil-grade quartz windows. The oven temperature is controlled by a variable resistance and can be raised to about 500 K. The temperature can be controlled to a precision of about 2–3 K.

Radicals are produced by photolysis of an appropriate precursor with a Lambda Physik Model EMG 101 excimer laser, whose beam is sent lengthwise through the cell. The 248-nm output from the laser, which is coupled into the cell by a dichroic flat, was varied from 150 to 450 mJ/pulse. For the source of the  $\text{CH}_2\text{Cl}$  radicals, we employed the photolysis (4); to produce  $\text{CHCl}_2$  radicals, we photolyzed the corresponding iodide:



The concentrations of the radicals are monitored by absorption of an ultraviolet beam which is produced by a deuterium lamp, collimated by a short focal length lens, and counterpropagated through the cell relative to the laser beam.  $\text{CH}_2\text{Cl}$  was monitored at 215 nm and  $\text{CHCl}_2$  at 210 and 220 nm, where their absorption cross-sections have been previously determined.<sup>14</sup> The lamplight that passes through the cell is focused onto the slits of a monochromator, and the light level is monitored as a function of wavelength by a photomultiplier tube. The photomultiplier output signal is followed in real time on a digital storage oscilloscope. The data are subsequently transferred to a microcomputer for storage, averaging, and analysis.

The gas mixtures are prepared in an all-Teflon-and-glass vacuum line and are passed into the cell via Teflon tubing. The gas flows are maintained and measured by Tylan flow controllers, which are periodically recalibrated. The pressure in the cell is measured by a MKS Baratron 1000-Torr pressure gauge. Radical precursor species are introduced into the gas mixture by passing a slow flow of nitrogen through a bubbler containing  $\text{CHCl}_2\text{Br}$  or  $\text{CH}_2\text{ClI}$  cooled in a water-ice bath. Typical flows for these

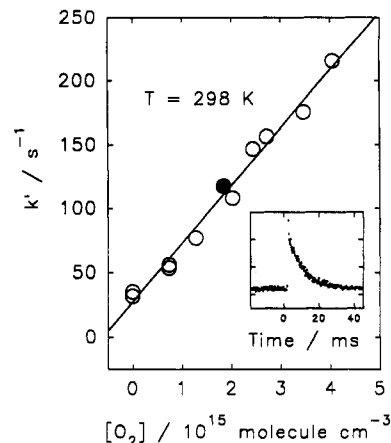


**Figure 1.** Exponential decay constants of  $\text{CHCl}_2^+$  ion signals ( $k^1$ ) vs  $[\text{O}_2]$  for a set of experiments conducted at 298 K. The inset is actual ion-signal profile recorded during one of the experiments whose decay constant is plotted here (dark circle). For this experiment,  $[\text{O}_2] = 1.84 \times 10^{15}$  molecule  $\text{cm}^{-3}$ .  $k^1 = 118 \pm 3 \text{ s}^{-1}$ . The line through the data is the exponential function fitted to the data.

experiments are several liters per minute at ambient pressure and several hundred cubic centimeters per minute at the lowest pressures studied (20 Torr). Given the small volume of the cell ( $<100 \text{ cm}^3$ ), we operate the laser at repetition rates of 0.1–0.5 Hz to ensure that the gas mixture is replenished between each flash. A typical experiment requires between 200 and 1000 laser shots to obtain a satisfactory signal-to-noise ratio.

The radical precursors,  $\text{CHCl}_2\text{Br}$  (Aldrich, purity  $>98\%$ ) and  $\text{CH}_2\text{ClI}$  (Aldrich, purity of  $97\%$ ) were degassed before use; oxygen (AGA Gaz spéciaux, purity  $>99.995\%$ ), nitrogen (AGA Gaz spéciaux, purity  $>99.995\%$ ), and synthetic air (AGA gaz spéciaux, purity the same as for  $\text{N}_2$  and  $\text{O}_2$ ) were used as supplied.

## Results

**A. Results of the Low-Pressure Experiments.** Molecular oxygen was always present in great excess over the alkyl radical concentration, resulting in pseudo-first-order kinetics. An exponential decay constant,  $k^1$ , was obtained for each radical-decay profile using a nonlinear least-squares analysis program. Bimolecular rate constants for reactions 1 and 2 were obtained from slopes of plots of  $k^1$  against  $[\text{O}_2]$ . The linear regression fit was weighted by the statistical uncertainties associated with the measured values of  $k^1$  and by the uncertainties on the bimolecular rate constant calculated using the largest of the internal and external errors.<sup>15</sup> The fitted intercepts for these linear regressions were always close to the measured wall-loss rate constant, which was determined in the absence of  $\text{O}_2$  before each set of experiments, demonstrating the validity of the pseudo-first-order analysis. A typical ion-signal-decay profile and decay-constant plot from one set of experiments to measure  $k^1$  for reaction 1 are shown in Figure 1. The bimolecular rate constants obtained and the experimental conditions used for the measurements are listed in Tables I and II and plotted, together with the results at higher pressures as falloff curves in Figures 2 and 3. In addition, we present together the results of the room-temperature experiments for reaction 1 conducted separately in helium and in nitrogen in Figure 4, where the difference in the third-body efficiencies of the two bath gases is highlighted.

**B. Results of the High-Pressure Experiments.** This series of experiments was also conducted under conditions where the concentration of  $\text{O}_2$  in the cell was sufficiently elevated to ensure pseudo-first-order loss of the alkyl radical signal. The details of the rate-constant extraction procedure are given below separately for reactions 1 and 2. In both cases, the experimental traces were analyzed by a nonlinear least-squares optimization program that includes differential equations to describe the set of possible

**TABLE I: Conditions and Results of Laser Photolysis/Photoionization Mass Spectrometry Experiments for Reaction 1**

T/K	M	[M]/ 10 <sup>16</sup>	10 <sup>-13</sup> [CHCl <sub>2</sub> Br] <sup>a</sup>	10 <sup>-15</sup> [O <sub>2</sub> ] <sup>a</sup>	k <sub>w</sub>	10 <sup>14</sup> k <sub>1</sub> <sup>b</sup>	no. of expts
298	N <sub>2</sub>	6.33	1.50	0.45–3.36	35	7.3 ± 0.3	7
298	N <sub>2</sub>	6.33	1.50	0.45–3.36	51	7.6 ± 0.3	7
298	N <sub>2</sub>	12.8	0.95	0.37–1.96	40	13.1 ± 0.5	7
298	N <sub>2</sub>	19.3	1.72	0.26–1.22	29	17.6 ± 0.6	7
298	N <sub>2</sub>	26.1	1.22	0.39–1.57	34	20.3 ± 0.5	6
298	He	3.06	1.64	0.57–2.03	28	1.9 ± 0.3	4
298	He	6.38	0.96	0.55–4.05	34	4.4 ± 0.3	11
298	He	12.8	1.64	0.87–5.02	28	6.8 ± 0.3	7
298	He	25.8	1.99	0.58–2.15	29	12.5 ± 0.5	6
333	N <sub>2</sub>	6.35	1.02	0.54–4.20	19	5.9 ± 0.2	7
333	N <sub>2</sub>	12.8	1.87	0.38–2.98	22	9.0 ± 0.5	6
333	N <sub>2</sub>	19.4	1.33	0.34–1.90	28	11.5 ± 0.3	7
333	N <sub>2</sub>	23.0	1.25	0.39–1.75	31	13.0 ± 0.7	6
383	N <sub>2</sub>	5.67	2.09	1.20–5.11	21	2.9 ± 0.1	7
383	N <sub>2</sub>	11.8	1.24	2.28–5.79	33	4.4 ± 0.2	5
383	N <sub>2</sub>	19.3	1.35	0.75–3.09	34	7.0 ± 0.3	6
383	N <sub>2</sub>	23.9	1.66	0.49–2.56	39	7.4 ± 0.5	5

<sup>a</sup> Units are molecules cm<sup>-3</sup>. <sup>b</sup> Units are cm<sup>3</sup> molecule<sup>-1</sup> s<sup>-1</sup>; uncertainties are 1σ statistical limits based on experimental precision.

**TABLE II: Conditions and Results of Laser Photolysis/Photoionization Mass Spectrometry Experiments for Reaction 2**

T/K	[N <sub>2</sub> ]/ 10 <sup>16</sup>	10 <sup>-13</sup> [CH <sub>2</sub> ClBr] <sup>a</sup>	10 <sup>-15</sup> [O <sub>2</sub> ] <sup>a</sup>	k <sub>w</sub> <sup>b</sup>	10 <sup>14</sup> k <sub>2</sub> <sup>c</sup>	no. of expts
298	6.32	3.18	0.57–1.87	24	11.2 ± 0.4	12
299	12.7	2.44	0.35–1.76	23	17.3 ± 0.9	11
301	12.6	5.43	0.48–1.48	23	18.7 ± 1.1	4
300	19.1	2.52	0.21–1.30	30	23.4 ± 0.8	7
297	25.8	2.85	0.20–1.11	37	27.4 ± 1.7	10
333	5.60	2.43	1.01–2.42	19	7.6 ± 0.4	7
333	12.8	2.60	0.34–1.91	21	13.0 ± 0.7	7
333	19.4	3.34	0.26–1.61	28	17.7 ± 0.9	7
333	23.1	2.59	0.26–1.75	26	19.6 ± 0.8	7
382	6.14	2.34	0.44–3.40	19	5.1 ± 0.4	5
382	12.5	2.56	0.77–2.64	26	8.3 ± 0.3	6
382	19.1	2.49	0.43–3.16	27	11.9 ± 0.5	6
382	23.9	2.58	0.46–2.15	28	14.1 ± 0.5	6
448	5.81	2.40	1.00–4.39	40	3.0 ± 0.2	6
448	12.8	2.68	0.59–3.56	48	5.8 ± 0.6	6
448	19.1	2.31	0.38–3.72	34	7.3 ± 0.6	8

<sup>a</sup> Units are molecules cm<sup>-3</sup>. <sup>b</sup> Units are s<sup>-1</sup>. <sup>c</sup> Units are cm<sup>3</sup> molecule<sup>-1</sup> s<sup>-1</sup>; uncertainties are 1σ statistical limits based on experimental precision.

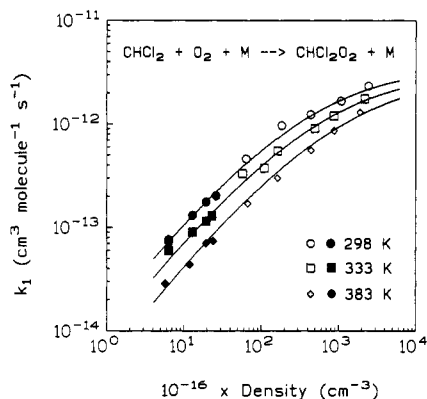


**Figure 2.** Pressure dependence of  $k_1$  obtained by both low-pressure experiments (filled symbols) and high-pressure experiments (open symbols). Bath gas is N<sub>2</sub>. The solid lines represent the RRKM fitting to the data; the RRKM results are given in Table VIII.

reactions of the system, even if these processes contribute negligibly to the kinetics in the presence of elevated oxygen concentrations. The motivation to develop a complete kinetic model is 2-fold: By the UV absorption technique, the radical precursor and products

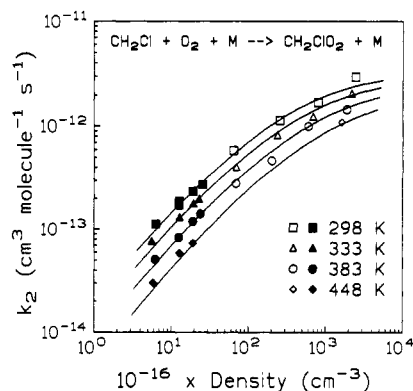


**Figure 3.** Pressure dependence of  $k_2$  obtained by both low-pressure experiments (filled symbols) and high-pressure experiments (open symbols). Bath gas is N<sub>2</sub>. The solid lines represent the RRKM fitting to the data; the RRKM results are given in Table VIII.

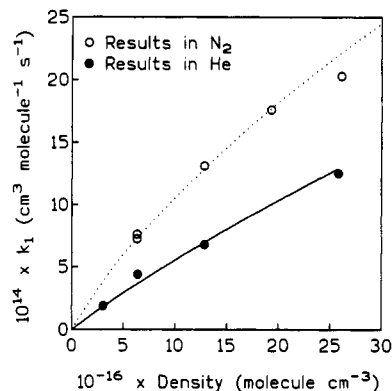
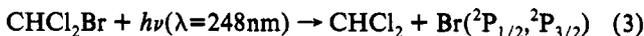


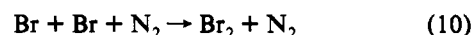
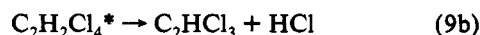
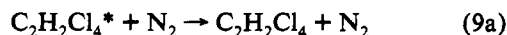
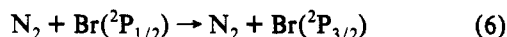
**Figure 4.** Comparison of our low-pressure determinations of  $k_1$  as observed in the two bath gases studied at 298 K. The dashed line represents the Troe expression fitting reported in Table VIII. The solid line gives the Troe expression optimization for the reaction in He, which yielded the value of  $6.4 \times 10^{-31}$  cm<sup>6</sup> molecule<sup>-2</sup> s<sup>-1</sup> for  $k_0$  with that bath gas.

of the reaction can absorb significantly at the observing wavelength, and therefore changes in their concentrations must also be taken into account. As we demonstrated in an earlier paper,<sup>7</sup> a complete model allows for a careful assessment of the effects of secondary chemical processes that might pose difficulty due to the relatively elevated initial radical concentrations by this technique (in particular, we are concerned about those reactions involving the halogen atoms formed in the flash).

**B.1. Photolysis of CHCl<sub>2</sub>Br.** It has been determined in previous studies that the photolysis of CHCl<sub>2</sub>Br near 250 nm yields CHCl<sub>2</sub> and Br atoms, the latter in a mixture of spin-orbit states:<sup>16,17</sup>



At elevated nitrogen pressures (i.e., near 760 Torr), the Br(<sup>2</sup>P<sub>1/2</sub>) is quenched faster than the time resolution of the apparatus,<sup>18</sup> and so the following set of recombination reactions is expected after the laser flash:



The competition between processes 9a and 9b has been studied at least twice previously as a function of pressure.<sup>14,19</sup> C<sub>2</sub>HCl<sub>3</sub> is known to have a very large absorption cross-section at 215

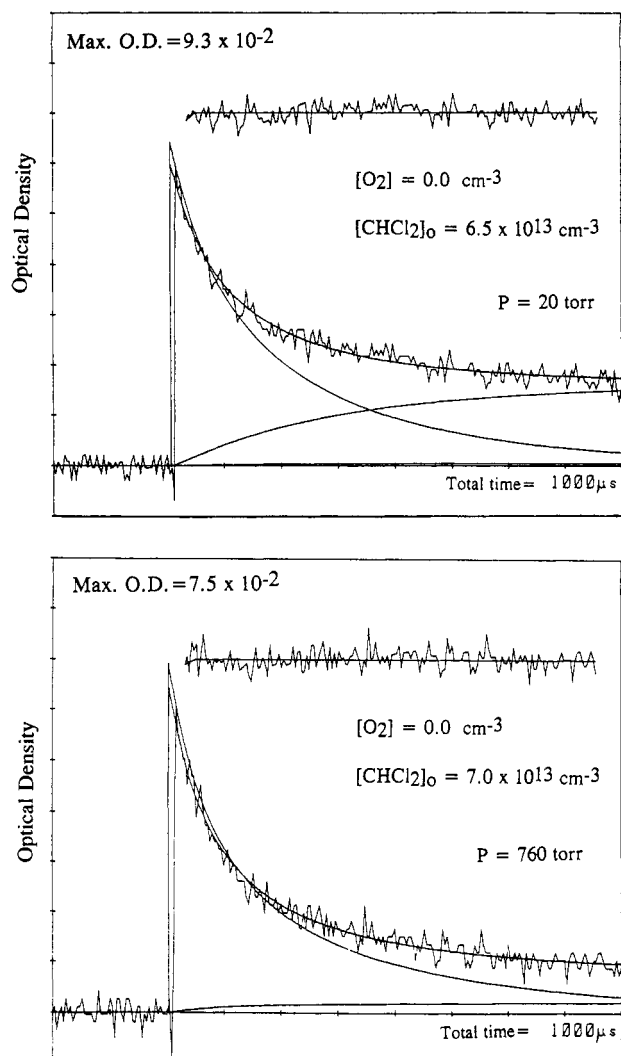
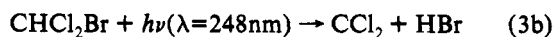


**Figure 5.** Time-absorption profiles as a function of pressure,  $\lambda = 215$  nm, showing the decay of  $\text{CHCl}_2$  in the absence of  $\text{O}_2$ . The experiments were conducted at 298 K. The lines that pass through the data represent the optimized fitting to the  $\text{CHCl}_2$  concentration as a function of time according to the kinetic model outlined in Table III. The lines passing underneath the data show the absorption contributions of individual species. The feature at the top of each trace shows the residual to the fitting.

nm,<sup>14</sup> and so as the pressure of the system is reduced, an increase in the observed residual absorption is expected as the ratio  $k_{9a}/k_{9b}$  decreases. In Figure 5, absorption-time profiles for the above chemical system are shown for experiments conducted at 20 and 760 Torr, and the increase of the residual absorption at low pressures is apparent. With the system of chemical equations given above, it was not possible to explain the extent of the rise of the residual absorption at low pressures. We considered two hypotheses for this phenomena.

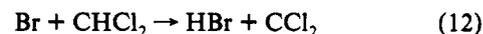
(1) There may be a significant production of  $\text{CCl}_2$  in the laser flash, which can recombine with the  $\text{CHCl}_2$  radical to form the highly absorbing species  $\text{C}_2\text{HCl}_3$ :



This process may become relatively more important at lower pressures if the rate constant for the recombination reaction between Br atoms and  $\text{CHCl}_2$  (reaction 7) falls off significantly over the pressure range or if there is a pressure dependence for reaction 3b.

(2) There may be a reaction between the Br atoms and  $\text{CHCl}_2$  which leads to the production of  $\text{CCl}_2$ , again followed by reaction

11 to give a species that is highly absorbing at 215 nm:

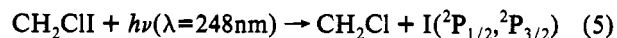


The increase in residual absorption at low pressures can be rationalized by a model where  $k_{12}$  remains constant as the total pressure is reduced, while the three-body recombination rate for the reaction between Br atoms and  $\text{CHCl}_2$ ,  $k_7$ , decreases over the experimental pressure range.

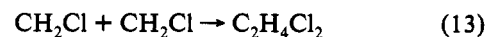
We have only indirect experimental evidence that little  $\text{CCl}_2$  is produced directly in the laser flash. With the determined  $\sigma(248)$  of  $\text{CHCl}_2\text{Br}$ , for a given laser-pulse energy we can estimate the yield of  $\text{CHCl}_2$  per photon absorbed. We find that the observed initial concentration of  $\text{CHCl}_2$  corresponds to a yield of one alkyl radical per photon absorbed (with an uncertainty of 20%) on the basis of the cross-section for  $\text{CHCl}_2$  given in Table III. In addition, we observed no change in this yield as a function of pressure. In order for reactions of  $\text{CCl}_2$  to play a role in the observed kinetics, an elevated yield of  $\text{CCl}_2$  is probably required due to the relative unreactive nature of ground-state halogenated carbene species.<sup>20,21</sup> If in fact the pressure-dependent residual absorption shown in Figure 5 is due to a  $\text{CCl}_2$  reaction, then the source of  $\text{CCl}_2$  is most likely a radical-radical reaction between species formed in the flash.

The experiments which we report are unable to resolve the ambiguity. All the experimental traces for the determination of  $k_1$  were analyzed using the parameters outlined in Table III, which correspond to the second hypothesis. We develop further the argument for this picture in the Discussion. There is a point of practice that needs to be underlined: the purpose for determining  $k_7$  is to characterize the secondary chemistry that can potentially interfere with the measurement of  $k_1$ . However, with the elevated oxygen concentrations employed for the majority of those experiments, the  $k_1$  optimization was insensitive to the model selected for the Br atom reactions. Excluding these secondary reactions entirely from the analysis raises the optimized values for  $k_1$  by less than 10% for most of the experimental determinations.

**B.2. Photolysis of  $\text{CH}_2\text{ClI}$ .** The bromide that is used as a  $\text{CH}_2\text{Cl}$  source in the low-pressure experiments,  $\text{CH}_2\text{ClBr}$ , could not be employed as a radical precursor in the high-pressure measurements because of its relatively large absorption cross-section near 215 nm. For these experiments, we used the corresponding iodide as the photolytic precursor. On the basis of the photolysis of similar halogen-substituted methanes, we expect the following process to be dominant at 248 nm:<sup>14,22,23</sup>



In the absence of oxygen, it was found that the loss of  $\text{CH}_2\text{Cl}$  radicals was rapid and could be well described by a second-order removal process at all the temperatures and pressures studied. A representative decay trace for this process is given in Figure 6. The following simple set of kinetic processes were used to model the recombination kinetics for the experiments conducted in the absence of oxygen:



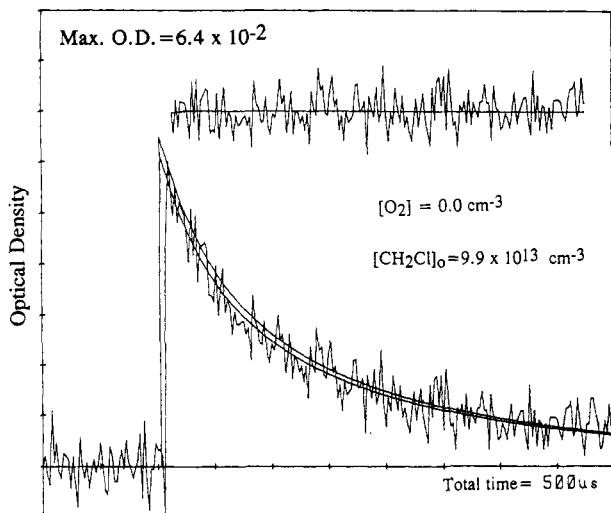
The rate constants for reactions 13 and 15 have been determined in previous studies.<sup>14,24</sup> Neither of these two reactions is sufficiently rapid to account for the observed loss of the  $\text{CH}_2\text{Cl}$  radical. We attribute the loss almost entirely to the recombination reaction (14); a value for  $k_{14}$  is determined from the nonlinear least-squares fitting procedure under each combination of pressure and temperature before oxygen is added to the cell. Given the simplified nature of the set of equations selected to represent the

**TABLE III: Values of Kinetic and Spectral Parameters Used in the Analysis of the High-Pressure Experiments for Reaction 1**

reaction	$k/(\text{cm}^3 \text{ molecule}^{-1} \text{ s}^{-1})$	ref
CHCl <sub>2</sub> + CHCl <sub>2</sub> → products	$9.3 \times 10^{-12}(T/298)^{-0.74}$	14
$k_{9a}/k_{9b}$	0.0 (at 760 Torr) 1.0 (at 20 Torr)	14
CHCl <sub>2</sub> + Br + M → CHCl <sub>2</sub> Br + M	$7.0 \times 10^{-11}$ (at 298 K, 760 Torr)	optimized parameter
CHCl <sub>2</sub> + Br → CCl <sub>2</sub> + HBr	$6.5 \times 10^{-11}$	assumed mechanism (see text)
CCl <sub>2</sub> + CHCl <sub>2</sub> → C <sub>2</sub> HCl <sub>3</sub> + Cl	$1.0 \times 10^{-11}$	assumed mechanism
Br + Br + M → Br <sub>2</sub> + M	$4.08 \times 10^{-34}[M]$	24
Br <sub>2</sub> + M →	$\exp\{1.70/RT\}$	
CHCl <sub>2</sub> + O <sub>2</sub> + M → CHCl <sub>2</sub> O <sub>2</sub> + M	see Table IV	optimized parameter

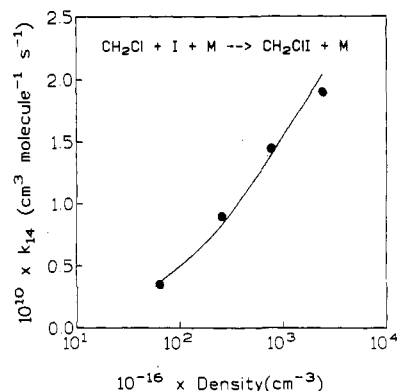
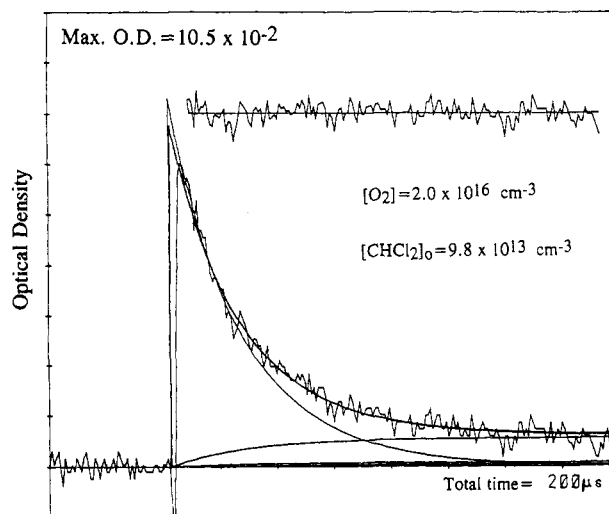
## Cross-Sections for Analysis

species	$\sigma(215)^a$	ref
CHCl <sub>2</sub>	$1.7 \times 10^{-17}$	14
C <sub>2</sub> H <sub>2</sub> Cl <sub>4</sub>	$2.0 \times 10^{-20}$	14
C <sub>2</sub> HCl <sub>3</sub>	$1.8 \times 10^{-17}$	14
CHCl <sub>2</sub> O <sub>2</sub>	$2.5 \times 10^{-18}$	determined in this work
CHCl <sub>2</sub> Br	$1.0 \times 10^{-18}$	determined in this work

<sup>a</sup> Units are cm<sup>2</sup> molecule<sup>-1</sup>.**Figure 6.** Time-absorption profile,  $\lambda = 210$  nm, showing the decay of CH<sub>2</sub>Cl in the absence of O<sub>2</sub>, conducted at 298 K. The line that passes through the data represents the optimized fitting to the CHCl<sub>2</sub> concentration as a function of time after compensating for the small amount of the precursor photolyzed in the laser flash. The feature at the top of the trace shows the residual to the fitting.

kinetics, the value of  $k_{14}$  is not easily interpreted, especially at low pressures; this is a topic we develop further in the Discussion. As we mentioned in an earlier publication, the observed loss for this sort of process may be influenced by spin-orbit quenching at pressures where the quenching is slow compared to the response time of the apparatus (about 5  $\mu$ s). The purpose of the fitting is to empirically determine the second-order rate of loss of CH<sub>2</sub>-Cl in the absence of O<sub>2</sub>, so that this value can be included in the fitting of the experiments conducted in the presence of O<sub>2</sub>. As is the case for the CHCl<sub>2</sub> system reported above, the determination of  $k_2$  is insensitive to large uncertainties in the rate coefficients for the secondary chemistry because of the elevated O<sub>2</sub> concentrations employed in the majority of the determinations. The values measured for  $k_{14}$  are shown graphically for the room-temperature experiments in Figure 7.

**B.3. Kinetics of Reaction 1.** In the presence of O<sub>2</sub>, the loss of the CHCl<sub>2</sub> is due predominantly to the reaction with O<sub>2</sub>, present in the cell in large excess. As discussed above, including the

**Figure 7.** Results for  $k_{14}$  as a function of pressure at 298 K. The solid line represents a fitting to the data using the Troe expression. From this,  $k_0 = 9.5 \times 10^{-29} \text{ cm}^6 \text{ molecule}^{-2} \text{ s}^{-1}$  and  $k_{\infty} = 3.4 \times 10^{-10} \text{ cm}^3 \text{ molecule}^{-1} \text{ s}^{-1}$ . The nature of the falloff is discussed in the text.**Figure 8.** A typical time-absorption profile of a kinetics experiment for reaction 1, for which  $\lambda = 215$  nm, at 298 K and in 760 Torr of total pressure. In addition to the rapid decay of the CHCl<sub>2</sub> signal, a residual absorption due to the formation of CHCl<sub>2</sub>O<sub>2</sub> is apparent. The total absorption is optimized using the simulation parameters given in Table III and includes a correction for the small amount of precursor photolyzed in the laser flash. The feature at the top shows the residual to the optimization.

background loss of CHCl<sub>2</sub> in the kinetic model results in values for  $k_1$  that are only slightly smaller than if this more complicated kinetic model is not employed. In Figure 8, we show the time-absorption profile of a typical experiment, in which the CHCl<sub>2</sub> signal decays on the microsecond time scale into a residual feature that is due to the absorption of CHCl<sub>2</sub>O<sub>2</sub>. In order to extract values of  $k_1$ , the experimental trace is nonlinear least-squares fitted to the complete kinetic model outlined in Table III by an optimization of  $k_1$ . The validity of employing a kinetic model that takes into account the secondary losses for CHCl<sub>2</sub> is supported by the results presented in Table IV, where it can be seen that, for a given pressure and temperature, there is no systematic dependence of  $k_1$  on the [O<sub>2</sub>], the latter often varied by a large factor. In addition to the results, the experimental conditions for the high-pressure determination of  $k_1$  are summarized in Table IV.

In a final series of experiments, we monitored a signal at 338 nm due to the formation of BrO at very long times relative to the time scale of the CHCl<sub>2</sub> decay. In the presence of O<sub>2</sub>, within tens of microseconds after the laser flash, the CHCl<sub>2</sub> radical is converted into CHCl<sub>2</sub>O<sub>2</sub>, and the Br atoms remain unreacted. In the previous paper on the CCl<sub>3</sub> + O<sub>2</sub> reaction, we were able to correlate the production of BrO with the rate of loss of CCl<sub>3</sub>O<sub>2</sub>, and thus assign an estimate of  $6 \times 10^{-12} \text{ cm}^3 \text{ molecule}^{-1} \text{ s}^{-1}$  for

**TABLE IV: Conditions and Results of Laser Photolysis/UV Absorption Experiments for Reaction 1**

T/K	[M]/Torr	$10^{-13}[\text{CHCl}_2]_0^a$	$10^{-16}[\text{O}_2]^a$	$10^{13}k_1^b$	no. of expts
298	760	5.3–8.8	0.6–3.2	$23.5 \pm 1.7$	9
298	335	6.0–7.5	1.7–3.0	$16.7 \pm 1.7$	3
298	135	6.0–7.0	2.5–4.5	$12.3 \pm 1.2$	3
298	57	6.0–8.0	2.4–3.2	$9.7 \pm 0.9$	3
298	21	3.5–8.0	6.8–19.0	$4.6 \pm 0.4$	11
333	760	8.0–10.0	1.8–4.6	$17.6 \pm 1.0$	4
333	300	7.3	2.6–3.8	$12.0 \pm 1.2$	3
333	171	7.5–10.0	4.1–5.6	$9.1 \pm 0.3$	3
333	58	4.8–7.0	2.2–11.8	$5.5 \pm 0.4$	4
333	38	6.0–6.5	9.8–21.7	$3.8 \pm 0.3$	2
333	21	6.5–8.0	11.0–12.0	$3.3 \pm 0.2$	3
383	760	4.5	1.2–9.1	$13.1 \pm 0.5$	6
383	340	5.2	3.2–8.2	$8.5 \pm 0.3$	4
383	175	5.0–6.3	6.8–10.6	$5.6 \pm 0.3$	3
383	66	3.8	13.0–22.0	$3.0 \pm 0.2$	3
383	27	4.0	18.5–26.0	$1.7 \pm 0.1$	3

<sup>a</sup> Units are molecules  $\text{cm}^{-3}$ . <sup>b</sup> Units are  $\text{cm}^3 \text{molecule}^{-1} \text{s}^{-1}$ ; uncertainties are  $1\sigma$  statistical limits based on experimental precision.

the O atom abstraction from the  $\text{RO}_2$  species by a bromine atom.<sup>7</sup> We find for this system that there is a small signal at 338 nm that can be attributed to the BrO radical, but the signal is only about 40% of the BrO signal observed under similar conditions for the  $\text{CCl}_3\text{O}_2$  system. The qualitative conclusion that can be drawn is that the  $\text{CHCl}_2\text{O}_2 + \text{Br}$  reaction does produce BrO, but to a lesser extent than is observed for the  $\text{CCl}_3\text{O}_2 + \text{Br}$  reaction.

**B.4. Kinetics of Reaction 2.** The analysis of the experiments is in principle identical to that applied to the  $\text{CHCl}_2 + \text{O}_2$  time-absorption profiles. In this case we found that, at 215 nm, the ratio of the initial absorption, due to  $\text{CH}_2\text{Cl}$ , relative to the residual absorption, due to  $\text{CH}_2\text{ClO}_2$ , is much smaller than for reaction 1. This situation arises because the maximum in the chlorinated methyl radical spectra shifts sharply to shorter wavelengths for  $\text{CH}_2\text{Cl}$ , as compared to  $\text{CHCl}_2$  and  $\text{CCl}_3$ .<sup>14,25</sup> The latter two have UV spectra that peak near 215 nm, whereas the maximum in the spectrum for the former is near 205 nm. In addition, the alkylperoxy radicals with chlorinated methyl R groups have UV absorption spectra that become increasingly strong with decreasing Cl substitution.<sup>26</sup> In this study, we determined the  $\text{CH}_2\text{ClO}_2$  cross-section to be  $(4.1 \pm 0.8) \times 10^{-18} \text{ cm}^2 \text{ molecule}^{-1}$  at 210 nm by routinely calibrating the residual absorption against the initial signal and using the value  $\sigma(210)(\text{CH}_2\text{Cl}) = (8.4 \pm 1.2) \times 10^{-18} \text{ cm}^2 \text{ molecule}^{-1}$  at that wavelength.<sup>14</sup> This value of  $\sigma(\text{CH}_2\text{ClO}_2)$  is a factor of 1.7 and 2.6 greater than the corresponding cross-sections for  $\text{CHCl}_2\text{O}_2$  and  $\text{CCl}_3\text{O}_2$ , respectively, at 210 nm.<sup>5,26</sup> The best compromise between experimental sensitivity and large  $\sigma(\text{CH}_2\text{Cl})$  was found to be at 210 nm, but even at this wavelength the signals for this series of experiments are characterized by a pseudo-first-order decay of the  $\text{CH}_2\text{Cl}$  radical absorption into relatively strong residual absorption. The spectra of alkyl radicals are more strongly peaked than the alkylperoxy radicals, and by changing the experimental wavelength to 220 nm,  $\sigma(\text{CH}_2\text{Cl})$  becomes small ( $< 1 \times 10^{-18} \text{ cm}^2 \text{ molecule}^{-1}$ )<sup>14</sup> relative to  $\sigma(\text{CH}_2\text{ClO}_2)$ . This results in time-absorption traces with an initial feature that grows into a prominent residual absorption. These two kinds of experimental time-absorption profiles are shown in Figure 9.

Only those experiments conducted at 210 nm were used in the determination of  $k_2$ . The experimental traces collected at 220 nm serve as a strong confirmation that the chemical system is well-understood. The optimizations of  $k_2$  were carried out using the kinetic and spectral parameters given in Table V. The values returned for  $k_2$  tend to be less precise for the  $k_1$  measurements because the pseudo-first-order decay of the alkyl radical was partially "masked" in the determination of the former. The nonlinear least-squares fitting routine returned consistent values

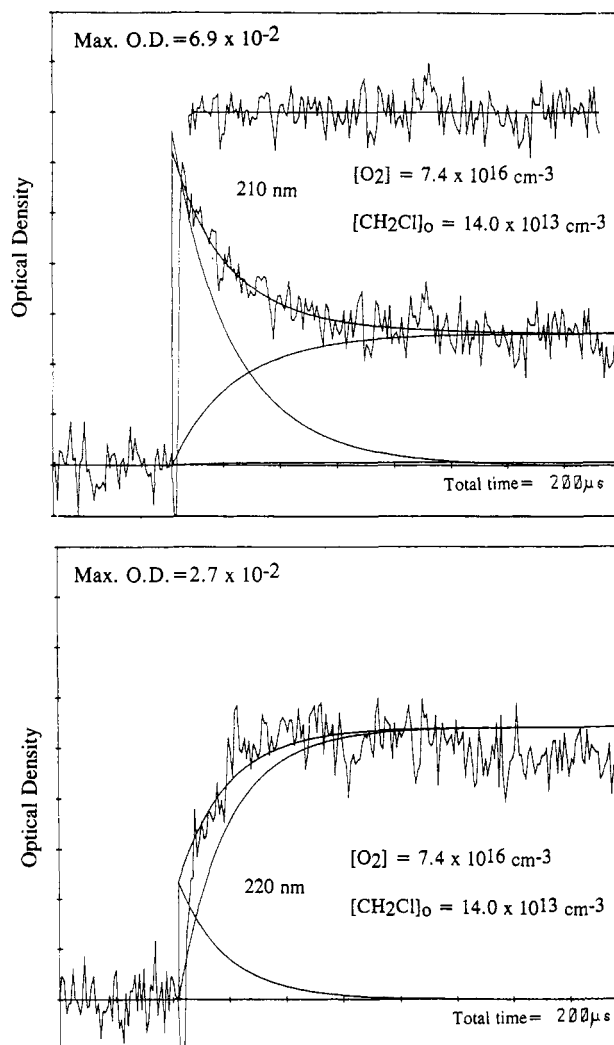


**Figure 9.** A typical time-absorption profile of a pair of kinetics experiments for reaction 2. In (a) the rapid decay of the  $\text{CHCl}_2$  signal into a large residual absorption, due to the formation of  $\text{CHCl}_2\text{O}_2$ , is apparent. In (b), the residual absorption becomes the dominant feature. The lines that pass through the data are the results of an optimized fitting using the kinetic and spectral parameters given in Table V.

**TABLE V: Values of Kinetic and Spectral Parameters Used in the Analysis of the High-Pressure Experiments for Reaction 2**

reaction	$k/(\text{cm}^3 \text{molecule}^{-1} \text{s}^{-1})$	ref	
$\text{CH}_2\text{Cl} + \text{CH}_2\text{Cl} \rightarrow \text{C}_2\text{H}_4\text{Cl}_2$	$2.8 \times 10^{-11}(T/300)^{-0.85}$	14	
$\text{CH}_2\text{Cl} + \text{I} + \text{M} \rightarrow \text{CH}_2\text{ClI} + \text{M}$	$1.9 \times 10^{-10}$ (at 298 K, 760 Torr) (see text and Figure 7 for details)	this work	
$\text{I} + \text{I} + \text{M} \rightarrow \text{I}_2 + \text{M}$	$6.51 \times 10^{-34}[\text{M}] \exp\{1.50/RT\}$	24	
$\text{CH}_2\text{Cl} + \text{O}_2 + \text{M} \rightarrow \text{CH}_2\text{ClO}_2 + \text{M}$	see Table VI	this work	
Cross-Sections for Analysis			
species	$\sigma(210)^a$	$\sigma(220)^a$	ref
$\text{CH}_2\text{Cl}$	$8.4 \times 10^{-18}$	$1.5 \times 10^{-18}$	14
$\text{C}_2\text{H}_4\text{Cl}_2$	$2.0 \times 10^{-20}$	$1.0 \times 10^{-20}$	14
$\text{CH}_2\text{ClO}_2$	$4.1 \times 10^{-18}$	$4.0 \times 10^{-18}$	determined in this work
$\text{CH}_2\text{ClI}$	$5.5 \times 10^{-19}$	$9 \times 10^{-20}$	determined in this work

<sup>a</sup> Units are  $\text{cm}^2 \text{ molecule}^{-1}$ .

for  $k_2$  over a significant range of experimental conditions, notably  $[\text{O}_2]$  and initial  $[\text{CH}_2\text{Cl}]$ , which gives us good confidence in the kinetic scheme employed in the analysis. The results and conditions for the high-pressure rate-constant determinations are summarized in Table VI and are shown graphically in Figure 3.

**TABLE VI: Conditions and Results of Laser Photolysis/UV Absorption Experiments for Reaction 2**

T/K	[M]/Torr	10 <sup>-13</sup> [CH <sub>2</sub> Cl] <sub>0</sub> <sup>a</sup>	10 <sup>-16</sup> [O <sub>2</sub> ] <sup>a</sup>	10 <sup>13</sup> k <sub>2</sub> <sup>b</sup>	no. of expts
298	760	8.5–12.0	0.8–2.8	29.5 ± 2.8	8
298	240	4.8–7.8	0.8–4.5	16.9 ± 1.7	6
298	80	6.3–8.0	3.0–7.0	11.4 ± 1.3	5
298	20	5.1–12.0	2.4–12.0	5.9 ± 0.7	11
333	760	8.5	1.3–3.0	20.5 ± 1.5	6
333	240	8.5	1.3–7.1	12.3 ± 1.4	4
333	83	7.2	2.9–9.5	8.2 ± 1.0	4
333	23	8.7–10.0	4.6–13.7	4.0 ± 0.4	4
383	760	6.3	0.8–3.3	14.5 ± 0.6	4
383	237	8.0	1.5–5.6	10.0 ± 0.9	4
383	80	6.3	5.7–11.2	4.7 ± 0.7	3
383	25	7.3	5.7–18.9	2.8 ± 0.4	4
448	760	6.1	1.5–3.1	11.0 ± 1.2	2

<sup>a</sup> Units are molecules cm<sup>-3</sup>. <sup>b</sup> Units are cm<sup>3</sup> molecule<sup>-1</sup> s<sup>-1</sup>; uncertainties are 1σ statistical limits based on experimental precision.

### Discussion

All the results of the rate-constant determinations for reactions 1 and 2 are shown in Figures 2 and 3. The curves that pass through the data represent a nonvariational RRKM fitting. This calculation was carried out using the program Falloff, which has been described recently in the literature,<sup>27</sup> and which is now available from Indiana University as Program Number QCMP 119. To briefly describe the approach, the program is used to calculate the dissociation rate constants for the appropriate RO<sub>2</sub> species, and these values are then multiplied by the value of the equilibrium constant for the reaction as determined by Russell et al., who made equilibrium measurements for this system over the temperature range 498–664 K.<sup>10</sup> From these determinations, Russell et al. were able to calculate a standard heat of reaction, ΔH°<sub>298</sub>, by using the third law analysis. The structural parameters for the alkyl and alkylperoxy radicals needed for the analysis were obtained by a theoretical calculation employing the BAC-MP4 method. Each RO<sub>2</sub> species has 2 stable rotational conformers, gauche and trans, and a set of 11 vibrational frequencies are given by Russell et al. for each conformer. The 12th internal degree of freedom was treated as a hindered rotor for which the reduced moment of inertia and the potential energy barrier are given for each conformer. The entropy value used in the thermodynamics calculation was taken to be the average of the two values calculated separately for the gauche and trans forms of the alkylperoxy radicals.

For the nonvariational RRKM calculation, the averages of the 11 highest vibrational frequencies for the 2 conformers were taken to represent the RO<sub>2</sub> vibrations, and the 12th degree of freedom was also treated as a vibration, the value for which was selected to reproduce the entropy as calculated from the equilibrium-constant determination. All of the structural parameters used in the calculations are given in Table VII. As the Lennard-Jones parameters for CHCl<sub>2</sub> and CH<sub>2</sub>Cl are unknown, we have used the values reported for the species CHCl<sub>3</sub> and CH<sub>2</sub>Cl<sub>2</sub> for these calculations.<sup>28</sup> In addition, the critical energy for dissociation of the RO<sub>2</sub> species, E°, is taken to be equal to the enthalpy change for the reaction at 0 K (ΔH°<sub>0</sub>), the assumption being that there is no potential barrier to reaction for these association reactions. The values of ΔH°<sub>0</sub> are obtained from the ΔH°<sub>298</sub> given by Russell et al., adjusted with calculated values for the heat capacities of these species.<sup>10</sup> These values are also reported in Table VII.

The "modified Gorin model" is adopted to describe the activated complex,<sup>29</sup> and the C–O stretch is assumed to be the reaction coordinate. There are seven vibration frequencies that are taken to be conserved degrees of freedom, equivalent to those for the alkyl radical and O<sub>2</sub>. The four deformation and torsional modes become two two-dimensional restricted rotors at the transition state; a hindrance parameter, η, takes into account the restriction

**TABLE VII: Spectroscopic and Structural Parameters Used in the RRKM Calculations**

parameter	CHCl <sub>2</sub> <sup>a</sup>	CH <sub>2</sub> Cl <sup>a</sup>	CHCl <sub>2</sub> O <sub>2</sub> <sup>b</sup>	CH <sub>2</sub> ClO <sub>2</sub> <sup>b</sup>	O <sub>2</sub> <sup>c</sup>
vibrational frequencies/cm <sup>-1</sup>	3062	3125	3039	3039	1580
	1227	2994	1331	2965	
	862	1382	1254	1464	
	720	976	1109	1352	
	539	778	1010	1243	
	290	447	823	1124	
			759	1028	
			510	960	
			395	766	
			288	471	
			249	314	
			34	30	
moments of inertia/(amu Å <sup>2</sup> )	10.88	1.83	137	18.96	11.7
	151.78	32.38	175.1	159.1	
	162.3	34.08	285.0	244.8	
Lennard-Jones σ <sup>d</sup> /Å <sup>2</sup>			5.39	4.89	
Lennard-Jones ε/k <sup>d</sup> /K			340.2	3533	
E°/cm <sup>-1</sup>			8569	9697	

<sup>a</sup> From ref 10. <sup>b</sup> Values taken from ref 10 and adjusted as described in text. <sup>c</sup> Reference 40. <sup>d</sup> Taken from representative compounds (see text and ref 28).

**TABLE VIII: Results of RRKM Calculations and Fittings to the Troe Expression for the Reactions CX<sub>3</sub> + O<sub>2</sub> + M → CX<sub>3</sub>O<sub>2</sub> + M**

A. RRKM Calculation Results					
CX <sub>3</sub>	k <sub>0</sub> <sup>a</sup>	n	k <sub>∞</sub> <sup>b</sup>	m	β <sub>c</sub>
CCl <sub>3</sub> <sup>c</sup>	1.1 × 10 <sup>-30</sup>	-5.3	3.5 × 10 <sup>-12</sup>	-1.0	0.15
CHCl <sub>2</sub>	1.8 × 10 <sup>-30</sup>	-4.2	3.3 × 10 <sup>-12</sup>	-1.0	0.38
CH <sub>2</sub> Cl	2.5 × 10 <sup>-30</sup>	-3.5	3.8 × 10 <sup>-12</sup>	-1.0	0.45
B. Troe Expression Fitting Results <sup>d</sup>					
CX <sub>3</sub>	k <sub>0</sub> <sup>a</sup>	n	k <sub>∞</sub> <sup>b</sup>	m	
CCl <sub>3</sub> <sup>c</sup>	(7.0 ± 0.2) × 10 <sup>-31</sup>	-6.3 ± 0.2	(2.6 ± 0.3) × 10 <sup>-12</sup>	-2.1 ± 0.6	
CHCl <sub>2</sub>	(12.6 ± 0.3) × 10 <sup>-31</sup>	-4.0 ± 0.2	(2.8 ± 0.2) × 10 <sup>-12</sup>	-1.4 ± 0.6	
CH <sub>2</sub> Cl	(18.8 ± 0.5) × 10 <sup>-31</sup>	-3.2 ± 0.2	(2.9 ± 0.2) × 10 <sup>-12</sup>	-1.2 ± 0.6	
CH <sub>3</sub> <sup>e</sup>	(10.0 ± 0.3) × 10 <sup>-31</sup>	-3.3 ± 0.4	(1.2 ± 0.2) × 10 <sup>-12</sup>	-1.2 ± 0.4	

<sup>a</sup> Units are cm<sup>6</sup> molecule<sup>-2</sup> s<sup>-1</sup>. <sup>b</sup> Units are cm<sup>3</sup> molecule<sup>-1</sup> s<sup>-1</sup>. <sup>c</sup> The average of several determinations, taken from ref 7. <sup>d</sup> Form of the expression from ref 31, for which F<sub>c</sub> = 0.6. <sup>e</sup> Taken from ref 33.

of the rotors. As the calculations are carried out using the modified strong collision hypothesis, the collisional efficiency β<sub>c</sub> is introduced to account for the falloff behavior.

The RRKM procedure calculates the third-order strong-collision rate constant, k<sub>0</sub><sup>sc</sup>, given the structural and thermodynamical parameters reported in Table VII. The parameters β<sub>c</sub> and η are adjusted at each temperature to obtain the best agreement between the calculated and experimental values. The resulting expressions for the high- and low-pressure limiting rate constants, k<sub>∞</sub> and k<sub>0</sub>, where k<sub>0</sub> = k<sub>0</sub><sup>sc</sup>β<sub>c</sub>, are reported in Table VIII, along with the values of β<sub>c</sub>.

In principle, the value of β<sub>c</sub> can be related to a value for ⟨ΔE⟩, the average energy transferred in collisions between the unimolecular reactant and the bath gas.<sup>30</sup> However, for kinetic data that are collected in the falloff pressure region, there is not sufficient precision in the determination of β<sub>c</sub> within the series to be able to draw firm conclusions. In particular, the RRKM calculation of k<sub>0</sub><sup>sc</sup> depends strongly on the value of the ΔH°<sub>298</sub> determined previously. We have found that a change in ΔH°<sub>298</sub> to its reported uncertainty limit results in a calculated value of k<sub>0</sub><sup>sc</sup> that in turn changes by a factor of 2.

The important conclusion that can be drawn from the RRKM calculation is that the thermodynamic parameters for these reactions as determined from the equilibrium study by Russell et al. taken together with these new kinetic data over a large

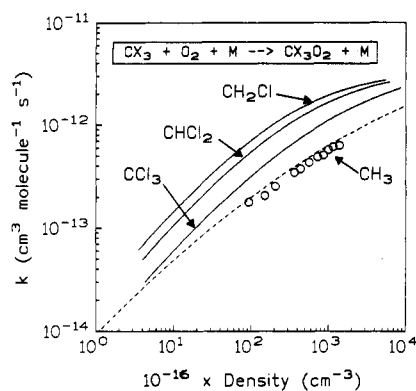


**Figure 10.** A comparison among the series of chlorinated methyl radical recombination reactions with molecular oxygen for the temperature 298 K. The lines representing the  $\text{CHCl}_2$  and  $\text{CH}_2\text{Cl}$  reactions are the RRKM fitting results reported in this work. The open circles are data from ref 32; the dashed line gives the recommended falloff curve for the  $\text{CH}_3$  reaction from ref 41; the  $\text{CCl}_3$  results are taken from ref 7.

range in pressure and temperature provide a complete and coherent picture of this important oxidation process. Along with the results of the RRKM calculation, in Table VIII are given the results of a weighted fitting of the Troe expression to the data set. For this fitting, we take the form that is recommended in ref 31, in which  $F_c$  is always taken to be 0.6, along with other approximations. From the optimized parameters quoted in Table VIII, values for  $k_1$  and  $k_2$  can be calculated for a wide range of pressure and temperature.

We can compare our results for reactions 1 and 2 with previous work on the  $\text{CH}_3$  and  $\text{CCl}_3$  reactions with  $\text{O}_2$ . In Figure 10, the room-temperature falloff curves determined here for the  $\text{CHCl}_2$  and  $\text{CH}_2\text{Cl}$  reactions are plotted along with our previous results on the  $\text{CCl}_3 + \text{O}_2$  reaction<sup>7</sup> and the results of Pilling and co-workers on the  $\text{CH}_3 + \text{O}_2$  reaction.<sup>32,33</sup> What we find is that, instead of falling between  $\text{CCl}_3$  and  $\text{CH}_3$  in reactivity with respect to association with  $\text{O}_2$ , the  $\text{CHCl}_2$  and  $\text{CH}_2\text{Cl}$  reactions are the fastest in the low-pressure limit. For  $k_0$ , we have the ordering  $k_0(\text{CH}_2\text{Cl}) > k_0(\text{CHCl}_2) > k_0(\text{CCl}_3) > k_0(\text{CH}_3)$ . In the high-pressure limit, it is difficult to draw conclusions from data that are gathered in the falloff region, but the extrapolations of the  $\text{CCl}_3$ ,  $\text{CHCl}_2$ , and  $\text{CH}_2\text{Cl}$  reaction-rate data give very similar values for  $k_\infty$  of about  $3.5 \times 10^{-12} \text{ cm}^3 \text{ molecule}^{-1} \text{ s}^{-1}$ . These are significantly faster than the high-pressure limiting rate constant reported by Pilling and co-workers for the  $\text{CH}_3 + \text{O}_2$  reaction of  $1.2 \times 10^{-12} \text{ cm}^3 \text{ molecule}^{-1} \text{ s}^{-1}$ .

With increasing substitution of chlorine atoms for hydrogen atoms in the methyl radical, there are two important trends in the series: (1) the C–O bond strength decreases,<sup>10</sup> and (2) the number of low vibrational frequencies increases. From our experimental observations, it appears that one chlorine atom on the methyl radical greatly enhances the low-pressure limiting rate constant because of the increase in the density of states due to the presence of low vibrational frequencies. Additional Cl atom substitution results in a subsequent reduction in the rate of association with  $\text{O}_2$ , suggesting that the  $\Delta H$  effect is more important than the relative gain in the density of states. We are currently conducting a variational RRKM calculation for the entire series in an attempt to understand this interesting trend in reactivity.

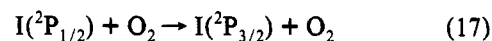
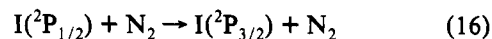
The results reported in this work also touch upon several secondary issues. The experiments conducted at low pressure at room temperature found a factor of 2 difference between the values for  $k_0$  in helium and in nitrogen, as shown in Figure 4. This ratio is, within experimental error, identical to the value that was determined for the ratio of collisional efficiencies in our previous study of the  $\text{CCl}_3 + \text{O}_2$  reaction.<sup>7</sup> The understanding of relative collisional efficiencies, and how they vary, can be useful for the

comparison of kinetic data collected at low pressures for three-body recombination reactions.<sup>13</sup>

The hypothesis of a H atom abstraction by Br as described by reaction 12 is entirely reasonable on the basis of the literature for this class of reaction.<sup>34</sup> Many of these are very slow near ambient temperatures because they are highly endothermic. On the basis of a recent value for the heat of formation of the  $\text{CCl}_2$  radical, the reaction is about 5 kcal/mol exothermic.<sup>35</sup> For the few well-studied cases where the H atom abstraction by Br is close to thermoneutral or exothermic, the rate of reaction can be quite rapid; two examples that can be cited are the H-abstraction reactions of Br with formaldehyde and with  $\text{HCO}$ .<sup>24</sup> The value for  $k_{12}$  used in the kinetic simulations of  $5 \times 10^{-11} \text{ cm}^3 \text{ molecule}^{-1} \text{ s}^{-1}$  seems reasonable for a reaction that is several kilocalories per mole exothermic.<sup>34</sup> As a final note on the issue of  $\text{CCl}_2$  formation via reaction 12, the  $\text{Br}(^2\text{P}_{1/2})$  that is quenched only slowly at low pressures in nitrogen has 10 kcal/mol of additional energy relative to  $\text{Br}(^2\text{P}_{3/2})$ , and thus the presence of excited-state Br atoms may contribute to the rise of the residual absorption as a function of pressure as shown in Figure 5.

From our observation of a peaked absorption at 338 nm,<sup>31</sup> we conclude that, at long times under our experimental conditions, there is a reaction between Br atoms and the  $\text{CHCl}_2\text{O}_2$  species that leads to the formation of BrO. We were surprised to find that the production of BrO in this system is less than half of what is observed under similar conditions for the  $\text{CCl}_3\text{O}_2 + \text{Br}$  reaction.<sup>7</sup> There are several possible explanations for this reduction in the signal, including the action of unforeseen secondary reactions that consume bromine-containing species under these experimental conditions. It is tempting to explain the discrepancy in terms of recent observations by Crowley and Moortgat,<sup>36</sup> and by Hayman et al.,<sup>37</sup> who have postulated the formation of ROOBr adducts when alkylperoxy radicals are formed in the presence of free bromine atoms. The BrO formation for the  $\text{CCl}_3\text{O}_2$  system appeared to be quantitative on the basis of a direct production mechanism.<sup>7</sup> If the ROOBr species which corresponds to the  $\text{CHCl}_2\text{O}_2$  radical is more stable, then perhaps the BrO formation is slowed or is in competition with a redissociation into the Br and  $\text{RO}_2$ . As was pointed out in the work on the  $\text{CCl}_3 + \text{O}_2$  reaction, this is more or less the chemical behavior that would be expected for a reaction that behaves analogously to the better studied  $\text{RO}_2 + \text{NO}$  reactions, which have been proposed to pass through a ROONO adduct whose fate is R group dependent.<sup>38</sup>

Our results on the recombination reaction between I atoms and  $\text{CH}_2\text{Cl}$  need to be interpreted with care. The situation is in fact similar to that reported for the  $\text{CCl}_3 + \text{Br}$  reaction, where a spin-orbit quenching step may influence the observed kinetics at low pressures in nitrogen.<sup>7</sup> The spin-orbit quenching of  $\text{I}(^2\text{P}_{1/2})$  is a well-studied process;<sup>23</sup> it has been found that  $\text{N}_2$  is a relatively inefficient spin-orbit quencher, whereas  $\text{O}_2$  is extremely efficient:



Deakin and Husain<sup>23</sup> have reported  $k_{16}^{298} = 7 \times 10^{-17}$  and  $k_{17}^{298} = 2 \times 10^{-11}$ , both in units of  $\text{cm}^3 \text{ molecule}^{-1} \text{ s}^{-1}$ . For those experiments conducted in the absence of  $\text{O}_2$ , the situation is further complicated by the presence of the radical precursor  $\text{CH}_2\text{ClI}$ ; halogenated alkyl species often act as very efficient quenchers of excited spin-orbit states of halogen atoms.<sup>23</sup> If the rates of I atom recombination with  $\text{CH}_2\text{Cl}$  for each spin-orbit state of I are significantly different, then the results shown in Figure 7 become difficult to interpret. In support of our observation of a large value for  $k_{14}$ , some previous work has been carried out on the recombination reactions between alkyl radicals and I atoms which show that these reactions can be quite rapid. For example, in an optoacoustical determination of the  $\text{CH}_2\text{I} + \text{I}$  three-body

recombination reaction, Hunter and Kristjansson reported a value of  $1 \times 10^{-10}$  cm<sup>3</sup> molecule<sup>-1</sup> s<sup>-1</sup> at 298 K and in 100 Torr of krypton.<sup>39</sup>

### Summary

The rate constants for the recombination reactions of the alkyl radicals CHCl<sub>2</sub> and CH<sub>2</sub>Cl with molecular oxygen have been measured by two techniques that offer complementary ranges of experimental pressures, and the agreement between the two techniques is excellent over the entire range of temperatures studied. In addition, we report the results of a nonvariational RRKM analysis that is based on structural and thermodynamic parameters for the reactions, determined in a previous study by experimental and ab initio techniques. With the theory, we were able to reproduce the observed variations in the rate constant for each reaction in terms of its overall magnitude, and of its pressure and temperature dependences.

**Acknowledgment.** Support for this research was provided by the National Science Foundation, Division of Chemical, Biological, and Thermal Engineering, under Grant CTS-89191704, and by the CEC (STEP Programme). We thank Irene R. Slagle for her advice and assistance.

### References and Notes

- (1) WMO Global Ozone Research and Monitoring Project, Report No. 20, 1989.
- (2) Senkan, S. M. *Detoxification of Hazardous Waste*; Exner, J. H., Ed.; Ann Arbor Science: Stoneham, MA, 1982; Chapter 3.
- (3) Copper, R.; Cumming, J. B.; Mulac, W. A. *Radiat. Phys. Chem.* **1980**, *16*, 169.
- (4) Ryan, K. R.; Plumb, I. C. *Int. J. Chem. Kinet.* **1984**, *16*, 591.
- (5) Danis, F.; Caralp, F.; Rayez, M. T.; Lesclaux, R. *J. Phys. Chem.* **1991**, *95*, 7300.
- (6) Ellermann, T. *A Spectrokinetic Laboratory Study of CCl<sub>3</sub> Reactions by Pulse Radiolysis*. Ph.D. Thesis, Riso National Laboratory Publication No. Riso-M-2932, 1991.
- (7) Fenter, F. F.; Lightfoot, P. D.; Niiranen, J. T.; Gutman, D. *Kinetics of the CCl<sub>3</sub> Association Reaction with Molecular Oxygen at 298 and 333K and from 1 to 760 torr Total Pressure*. Submitted for publication to *J. Phys. Chem.*
- (8) Russell, J. J.; Seetula, J. A.; Gutman, D.; Danis, F.; Caralp, F.; Lightfoot, P. D.; Lesclaux, R.; Melius, C. F.; Senkan, S. M. *J. Phys. Chem.* **1990**, *94*, 3277.
- (9) Caralp, F.; Lesclaux, R. *Chem. Phys. Lett.* **1983**, *102*, 54.
- (10) Russell, J. J.; Seetula, J. A.; Gutman, D.; Melius, C. F.; Senkan, S. M. *23rd Symposium on Combustion*; The Combustion Institute: Pittsburgh, PA, 1990; p 163.
- (11) Slagle, I. R.; Gutman, D. *J. Am. Chem. Soc.* **1985**, *107*, 5342.
- (12) Wagner, A. F.; Slagle, I. R.; Sarzynski, D.; Gutman, D. *J. Phys. Chem.* **1990**, *94*, 1853.
- (13) Gilbert, R. G.; Smith, S. C. *Theory of Unimolecular and Recombination Reactions*; Blackwell Scientific: London, 1990.
- (14) Roussel, P. B.; Lightfoot, P. D.; Caralp, F.; Catoire, V.; Lesclaux, R.; Forst, W. *J. Chem. Soc., Faraday Trans.* **1991**, *87*, 2367.
- (15) Cvetanovic, R. J.; Singleton, D. L.; Paraskevopoulos, G. *J. Phys. Chem.* **1979**, *83*, 50.
- (16) Okabe, H. *Photochemistry of Small Molecules*; John Wiley and Sons: New York, 1978.
- (17) Gibb, J. C.; Tedder, J. M.; Walton, J. C. *J. Chem. Soc., Perkin Trans. 2* **1974**, *68*, 807.
- (18) Donovan, R. J.; Husain, D. *Trans. Faraday Soc.* **1966**, *62*, 2987.
- (19) Kim, K. C.; Setser, D. W. *J. Phys. Chem.* **1974**, *78*, 2166.
- (20) Meunier, H.; Purdy, J. R.; Thrush, B. A. *J. Chem. Soc., Faraday Trans. 2* **1980**, *76*, 1304.
- (21) Tsee, J. J.; Wampler, F. B.; Rice, W. W., Jr. *Chem. Phys. Lett.* **1980**, *73*, 519.
- (22) Takacs, G. A.; Willard, J. E. *J. Phys. Chem.* **1977**, *81*, 1343.
- (23) Deakin, J. J.; Husain, D. *J. Chem. Soc., Faraday Trans. 2* **1972**, *68*, 41.
- (24) Westley, F.; Herron, J. T.; Hampson, R. F.; Mallard, W. G. *NIST Chemical Kinetics Database*; NIST Standard Reference Database 17; U.S. Department of Commerce: Washington, DC, April 1992.
- (25) Danis, F.; Caralp, F.; Veyret, B.; Loirat, H.; Lesclaux, R. *Int. J. Chem. Kinet.* **1989**, *21*, 715.
- (26) Catoire, V. Private communication on soon-to-be-published results.
- (27) Forst, W. *J. Chem. Soc., Faraday Trans. 2* **1988**, *84*, 569.
- (28) Svebla, R. A. *NASA Technical Report R132*; NASA: Washington, DC, 1962.
- (29) Davies, J. W.; Pilling, M. J. *Bimolecular Collisions: Advances in Gas Phase Photochemistry and Kinetics*; Ashfold, M. N. R., Baggott, J. E., Eds.; Royal Society of Chemistry: Herts, U.K., 1989.
- (30) Gardiner, W. C., Jr., Ed. *Combustion Chemistry*; Springer-Verlag: New York, 1984.
- (31) DeMore, W. B.; Sander, S. P.; Golden, D. M.; Molina, M. J.; Hampson, R. F.; Kurylo, M. J.; Howard, C. J.; Ravishankara, A. R. *Chemical Kinetics and Photochemical Data for Use in Stratospheric Modeling*; JPL Publication 90-1; 1990.
- (32) Pilling, M. J.; Smith, M. J. C. *J. Phys. Chem.* **1985**, *89*, 4713.
- (33) Keiffer, M.; Pilling, M. J.; Smith, M. J. C. *J. Phys. Chem.* **1987**, *91*, 6028.
- (34) Tschuikow-Roux, E.; Salomon, D. R.; Paddison, S. *J. Phys. Chem.* **1987**, *91*, 3037.
- (35) Paulino, J. A.; Squires, R. R. *J. Am. Chem. Soc.* **1991**, *113*, 5573.
- (36) Crowley, J. N.; Moortgat, G. K. *J. Chem. Soc., Faraday Trans.* **1992**, *88*, 2437.
- (37) Hayman, G. D.; Jenkin, M. E.; Murrells, T. P. *Eurotrac Annual Report: Commission of the European Communities*; Garmisch-Partenkirchen, 1990; Part 8.
- (38) Lightfoot, P. D.; Cox, R. A.; Crowley, J. N.; Destriau, M.; Hayman, G. D.; Jenkin, M. E.; Moortgat, G. K.; Zabel, F. *Atmos. Environ.* **1992**, *26A*, 1805.
- (39) Hunter, T. F.; Kristjansson, K. S. *J. Chem. Soc., Faraday Trans. 2* **1982**, *78*, 2067.
- (40) Stull, D. R.; Prophet, H. *JANAF Thermochemical Tables*, 2nd ed.; NSRDS-NBS 37; National Bureau of Standards: Washington, DC, 1971.
- (41) Atkinson, R. *Atmos. Environ.* **1990**, *24A*, 1.